CHIN. PHYS. LETT. Vol. 37, No. 10 (2020) 108401

Antimony Selenide Thin Film Solar Cells with an Electron Transport Layer of Alq_3

Wen-Jian Shi(师文建)[1], Ze-Ming Kan(阚泽明)[1], Chuan-Hui Cheng(程传辉)[2*], Wen-Hui Li(李文慧)[2], Hang-Qi Song(宋航琪)[2], Meng Li(李萌)[2], Dong-Qi Yu(于东麒)[1*], Xiu-Yun Du(杜秀云)[1], Wei-Feng Liu(刘维峰)[3], Sheng-Ye Jin(金盛烨)[4], and Shu-Lin Cong(丛书林)[2]

[1]*School of Physics and Electronic Technology, Liaoning Normal University, Dalian 116029, China*
[2]*School of Physics, Dalian University of Technology, Dalian 116024, China*
[3]*Mechanical and Electrical Engineering College, Hainan University, Haikou 570228, China*
[4]*State Key Laboratory of Molecular Reaction Dynamics, Dalian Institute of Chemical Physics, Chinese Academy of Sciences, Dalian 116023 China*

(Received 14 July 2020; accepted 31 August 2020; published online 29 September 2020)

We fabricated Sb_2Se_3 thin film solar cells using tris(8-hydroxy-quinolinato) aluminum (Alq_3) as an electron transport layer by vacuum thermal evaporation. Another small organic molecule of N,N'-bis(naphthalen-1-yl)-N,N'-bis(phenyl)benzidine (NPB) was used as a hole transport layer. We took ITO/NPB/Sb_2Se_3/Alq_3/Al as the device architecture. An open circuit voltage (V_{oc}) of 0.37 V, a short circuit current density (J_{sc}) of 21.2 mA/cm^2, and a power conversion efficiency (PCE) of 3.79% were obtained on an optimized device. A maximum external quantum efficiency of 73% was achieved at 600 nm. The J_{sc}, V_{oc}, and PCE were dramatically enhanced after introducing an electron transport layer of Alq_3. The results suggest that the interface state density at Sb_2Se_3/Al interface is decreased by inserting an Alq_3 layer, and the charge recombination loss in the device is suppressed. This work provides a new electron transport material for Sb_2Se_3 thin film solar cells.

PACS: 84.60.Jt, 85.30.De DOI: 10.1088/0256-307X/37/10/108401

Energy and environmental problems are serious concerns that have driven the urgent need to develop cheap and clean energy sources such as solar cells. Thin film solar cells based on CdTe and $CuIn_{1-y}Ga_ySe_2$ (CIGS) have achieved high power conversion efficiencies (PCEs) of more than 20%.[1,2] Yet, concerns remain on the scarcity of Te, the toxicity of Cd, and high price of In and Ga.[3] Hence, it is essential to find cheap, earth-abundant, and low-toxicity materials for applications in solar cells. In recent years, antimony selenide (Sb_2Se_3) has received considerable attention because of its low toxicity, earth abundance, suitable band gap (1.03 eV indirect and 1.17 eV direct),[4] high absorption coefficient ($>10^5$ cm^{-1} at around 600 nm),[5] single phase structure, and inert grain boundaries. In Sb_2Se_3 crystal, $(Sb_4Se_6)_n$ ribbons stack along the $\langle 001\rangle$ direction through strong covalent Sb–Se bonds, whereas the $(Sb_4Se_6)_n$ ribbons are held together by van der Waals forces in the $\langle 100\rangle$ and $\langle 010\rangle$ directions.[6] Various methods have been used to deposit Sb_2Se_3 thin films, such as vacuum thermal evaporation,[7] rapid thermal evaporation,[8] vapor transport deposition,[9,10] magnetron sputtering,[11,12] closed space sublimation,[13,14] electrodeposition,[15] and solution processing method.[16–21] The Sb_2Se_3 solar cell was first reported by Nair *et al.* in 2009, and the PCE was only 0.66%.[22] In past years, the device efficiency has been gradually improved. Luo *et al.*[7] fabricated a Sb_2Se_3 thin film solar cells with a PCE of 1.9% by vacuum thermal evaporation in 2014. In the same year, they improved the PCE to 3.7% by an additional selenization step.[23] In 2015, a PCE of 5.6% was obtained by Zhou *et al.* using the rapid thermal evaporation technique.[8] Choi *et al.*[16] have achieved a PCE of 6.4% via the solution processing method. In 2018, Wen *et al.*[9] achieved a PCE of 7.6% using the vapor transport deposition technique. A record PCE of 9.2% was created by Li *et al.* in 2019 using closed space sublimation.[24] This record efficiency of 9.2% is still much lower than its Shockley–Queisser limit of higher than 30%.[25–27] Therefore, further research is still required to improve the performance of the Sb_2Se_3 thin film solar cells.

The crystal grains sizes are relatively large in the polycrystal films fabricated by both the rapid thermal evaporation[8] and closed space sublimation.[13,14] However, the deposition rates are so high (∼8 nm/s) that the Sb and Se atoms cannot relax to their equilibrium sites, leading to the pinholes, defects, and wild orientations of the $(Sb_4Se_6)_n$ chains in different crystal grains. In term of the vapor transfer deposition,

Supported by the High Level Talents Project of Hainan Basic and Applied Research Program (Natural Science) (Grant No. 2019RC118), and the Open Fund of the State Key Laboratory of Molecular Reaction Dynamics in DICP (Grant No. SKLMRD-K202005).
*Corresponding authors. Email: chengchuanhui@dlut.edu.cn; useeu@163.com
© 2020 Chinese Physical Society and IOP Publishing Ltd

the optimized deposition rate is also very high.[9] The high deposition rate may result in the wild orientations of $(Sb_4Se_6)_n$ chains and bad quality of the film. Hydrothermal deposition technique[21] allows moderate experimental condition (135 °C) and low nucleation rate, which results in the large size of the crystal grains and good device performance. At present, for the films fabricated by the vacuum thermal evaporation followed post annealing, the crystal grains sizes are relatively small, and the preferred orientation of (020) is unfavored for the charge transport. However, the film with a preferred orientation of (001) and higher efficiency will be realized by the surface modification of substrate, introduction of buffer layer, and post treatment.

Sb_2Se_3 is a p-type semiconductor. Thus, the electron extraction is crucial for Sb_2Se_3 film solar cells. Numerous electron transport materials such as CdS,[7] Zn-doped CdS,[28] In-doped CdS,[29] ZnO,[30] TiO_2,[31] SnO_2,[32] and PCBM[33,34] have been used in Sb_2Se_3 thin film solar cells. Small organic molecules of tris(8-hydroxy-quinolinato) aluminum (Alq_3) are a famous electron transport material in organic light-emitting diodes, and can be easily deposited by vacuum thermal evaporation. In this work, we fabricated Sb_2Se_3 thin film solar cells using tris(8-hydroxy-quinolinato) aluminum (Alq_3) as an electron transport layer by vacuum thermal evaporation. Another small organic molecule of N,N'-bis(naphthalen-1-yl)-N,N'-bis (phenyl) benzidine (NPB) was used as a hole transport layer, and a PCE of 3.79% was achieved, which is much higher than that of the device without an Alq_3 layer. In most of the devices reported previously, transparent conductive oxide (TCO) is used as cathode, and noble metal Au is used as anode. However, TCO was used as anode in our device, and metal Al was used as a cathode, reducing the cost of the device.

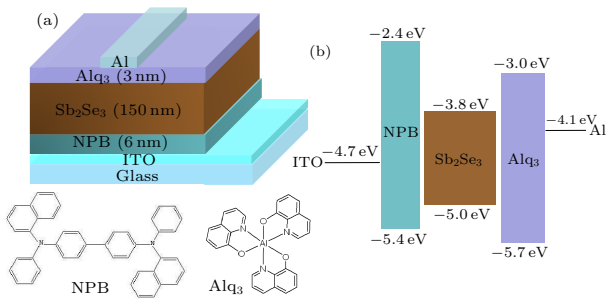

Fig. 1. (a) Device architecture and molecular structures. (b) Energy-level diagram of the device.

Sb_2Se_3 (99.99%) was purchased from Sigma. Alq_3 (sublimed grade, ≥99.0%) and NPB (sublimed grade, ≥99.0%) were purchased from Nichem Corp. Solar cells were fabricated by vacuum thermal evaporation ($<5.0 \times 10^{-4}$ Pa) on commercially patterned indium tin oxide (ITO) coated glass with a sheet resistance less than $8\,\Omega/cm^2$. Substrates were ultrasonically washed in acetone, alcohol and deionized water in sequence, and then dried by a flow of nitrogen gas. Next, NPB and Sb_2Se_3 were successively deposited by vacuum thermal evaporation. Then, vacuum was broken and substrates were transferred to a vacuum tube furnace with two temperature zones to anneal in the atmosphere of Se at 280 ℃ for 30 min, and was naturally cooled down to room temperature. During selenization the source of Se was kept at 210 ℃, and the nitrogen gas was introduced to tube with a flux of 30 sccm and a pressure of ∼35 Pa. After that, Alq_3, and Al electrode were successively deposited by vacuum thermal evaporation. A stainless shadow mask was used to define the device profile ($1.5 \times 5.0\,mm^2$). During vacuum evaporation, film thickness was monitored by a quartz crystal microbalance. The deposition rates were ∼ 0.2 nm/s for the organic and Sb_2Se_3 films. The device and molecular structures are shown in Fig. 1(a). A diagram of the device energy levels is depicted in Fig. 1(b). Transmittance measurements were conducted using a Shimadzu UV3600 spectrophotometer. X-ray diffraction (XRD) was performed on a Shimadzu XRD-6100. Scanning electron microscopy (SEM) images were obtained on a Zeiss SUPARR-5503040702. Atomic force microscopy images were obtained on a Bruker Dension Icon. The photovoltaic response was measured using a Keithley 2611A source meter under AM1.5 illumination from a Zolix Sirius-SS150A solar simulator (China) at a power density of $100\,mW/cm^2$. The irradiation intensity on the cells was adjusted by a standard calibrated Si solar cell. External quantum efficiency (EQE) was measured on a Zolix SCS100 analyzer. The capacitance-voltage (C–V) characteristics were measured on an Agilent B1500A semiconductor device analyzer in the darkness, where an alternating current voltage of 30 mV and direct current bias voltage varying from −0.8 V to 0.4 V were applied during the measurement. The transient photovoltage (TPV) signals were monitored by a Keysight DSOX3012 T digital oscilloscope. During the TPV measurement, the device was illuminated by laser pulses (532 nm, 5-ns width, 8 Hz, New Wave), and a background white light ($50\,mW/cm^2$) from a xenon lamp was used to hold the carrier density. All measurements were carried out at room temperature.

Figure 2(a) shows the transmittance spectrum of the Sb_2Se_3 film. The absorption of the Sb_2Se_3 film covers the ultraviolet, visible, and near-infrared regions. We obtained the optical band gap of the Sb_2Se_3 thin film using the following relation:

$$(\beta h\nu)^2 = A(h\nu - E_g), \tag{1}$$

where β is the absorption coefficient at a frequency of v, h is the Plank constant, E_g is the optical band gap, and A is a constant. The curve of $(\beta h\nu)^2$–$h\nu$ is given in the insert of Fig. 2(a), which exhibits a linear zone. An optical band gap of 1.25 eV is obtained from the

horizontal intercept, which is closed to the results reported by other groups.[4] Absorption spectra of NPB and Alq_3 films are shown in Fig. 2(b).

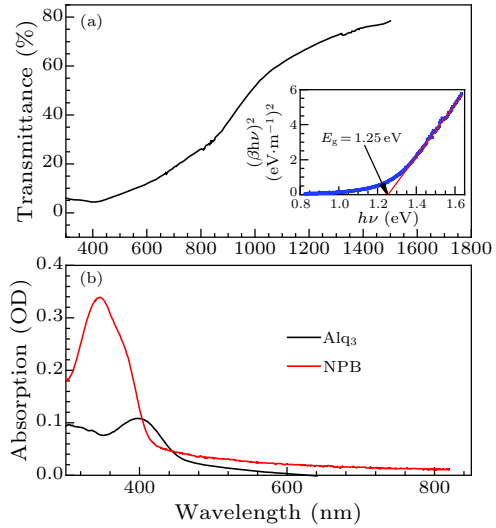

Fig. 2. (a) Transmission spectrum of the Sb_2Se_3 film. Inset: curve of $(\beta h\nu)^2$–$h\nu$ for the Sb_2Se_3 film. (b) Absorption spectra of NPB and Alq_3 film.

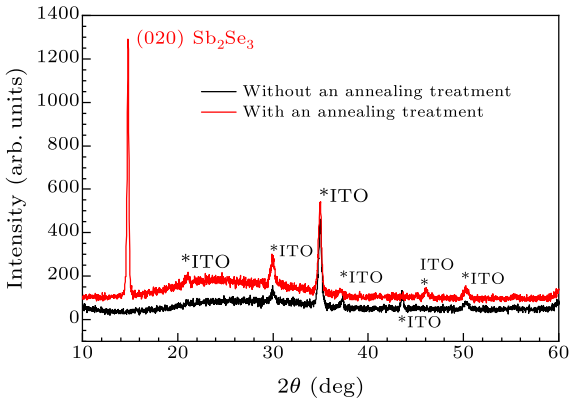

Fig. 3. XRD patterns of the Sb_2Se_3 film with and without an annealing treatment.

To characterize the crystal structure and surface morphology of the Sb_2Se_3 films we performed the XRD and SEM measurements. Figure 3 shows the XRD patterns of the Sb_2Se_3 film with and without an annealing treatment. For the film without an annealing process, no diffraction feature was observed, which indicated an amorphous film. Meanwhile, for the film with an annealing process, a strong $\langle 020 \rangle$ diffraction peak was observed at $2\theta = 14.9°$ with a full width at half maximum of 0.22 °C (JCPDS 15–0816). The XRD pattern shows no other diffraction peak, which indicates a preferred orientation of the $\langle 020 \rangle$ crystal plane. Figures 4(a)–4(d) display the SEM surface and cross-sectional images of the Sb_2Se_3 films with and without an annealing treatment. As can be seen, without an annealing treatment, the Sb_2Se_3 film exhibited a very smooth surface and cross section without any texture. However, for the Sb_2Se_3 film with an annealing treatment, grain boundaries are clearly observed, and textures are parallel to the film surface. We also observed that the texture directions vary from grain to grain. The sizes of some grains are more than 1 µm. AFM surface morphologies were also measured, and the images are shown in Figs. 4(e) and 4(f). The rms roughness of the Sb_2Se_3 films is slightly increased from 0.927 to 2.08 nm after an annealing treatment. The crystal grains are also observed after an annealing treatment, which are consistent with the SEM and XRD measurements. The results suggest that an annealing treatment can significantly improve the crystal quality of the Sb_2Se_3 film.

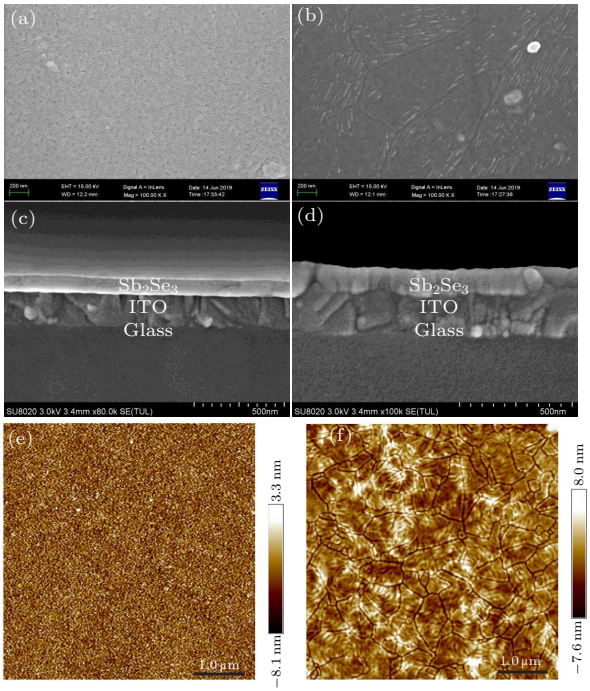

Fig. 4. [(a),(b)] SEM surface images and [(c),(d)] cross-sectional views of the Sb_2Se_3 films deposited on ITO coated glass substrates [(a),(c)] without and [(b),(d)] with an annealing treatment. AFM surface images of the Sb_2Se_3 film deposited on ITO coated glass substrates without (e) and with (f) an annealing treatment.

We next fabricated the solar cells with the architecture of ITO/NPB (6.0 nm)/Sb_2Se_3 (150 nm)/Alq_3 (3.0 nm)/Al. Here, NPB was used as a hole transport layer, and Alq_3 was served as an electron transport layer. We also prepared a controlled cell without an Alq_3 layer for comparison. The hole mobility of NPB varied from 1.63×10^{-5} to 7.64×10^{-4} $cm^{-2}{\cdot}V^{-1}{\cdot}s^{-1}$ as the film thickness increased from 50 to 1000 nm.[35] The electron mobility of Alq_3 is on an order of magnitude of 10^{-6} $cm^{-2}{\cdot}V^{-1}{\cdot}s^{-1}$.[36] The optimized thickness of NPB and Alq_3 less than 10 nm in the cell because of their low carrier mobilities. The J–V curves of the solar cells with and without the Alq_3 layer under one sun illumination (AM 1.5, 100 mW/cm^2) are shown in Fig. 5(a). Device performance parameters are summarized in Table 1. By introducing an electron

transport layer of Alq_3, the V_{oc}, J_{sc}, FF, and PCE of the device are significantly improved. An open circuit voltage (V_{oc}) of 0.37 V, a short circuit current density (J_{sc}) of 21.2 mA/cm^2, fill factor (FF) of 48%, and a PCE of 3.79% are obtained on an optimized device. The PCE was increased by 72% after introducing an Alq_3 layer.

Table 1. Summary of the cell performance parameters extracted from J–V curves.

Cell structure	V_{oc} (V)	J_{sc} (mA/cm^2)	FF	R_s (Ω/cm^2)	J_0 (mA/cm^2)	n	PCE
With Alq_3	0.37	21.2	0.48	2.18	8.9×10^{-3}	2.07	3.79%
Without Alq_3	0.30	18.2	0.40	2.37	1.4×10^{-2}	1.93	2.20%

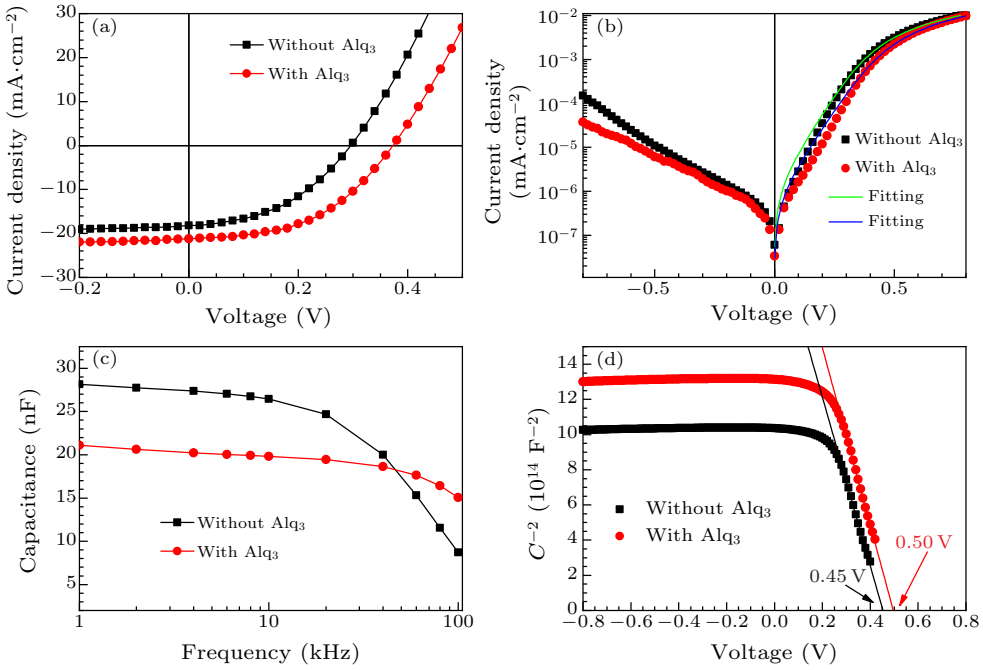

Fig. 5. J–V curves of solar cells with and without an Alq_3 layer (a) under light (AM 1.5, 100 mW/cm^2) and (b) in the darkness. (c) C–f and (d) C^{-2}–V characteristics of the device with and without an Alq_3 layer in the darkness.

To explain the enhanced performance by introducing an Alq_3 layer, we measured the J–V characteristics of the device with and without an Alq_3 layer in the darkness, and the results are given in Fig. 5(b). J of the device can be described by Eq. (2), which is the modified Shockley equation where a series resistance R_s is considered. Equation (3) can be easily deduced from Eq. (2), which suggests that a lower reverse saturation current density (J_0) means a higher V_{oc}.

$$J = J_0\left\{\exp\left[\frac{q(V - JR_s)}{nk_BT}\right] - 1\right\} - J_{ph}, \tag{2}$$

$$V_{oc} \approx \frac{nk_BT}{q}\ln\frac{J_{sc}}{J_0}, \tag{3}$$

where J_0 is the reverse saturation current density, q is the charge of an electron, n is the ideal factor, k_B is the Boltzmann constant, T is the temperature, and J_{ph} is the photo-current density. After introducing an Alq_3 layer, the current densities under reverse bias are decreased. The J–V curves are fitted with Eq. (2), and the fit parameters are given in Table 1. The J_0 are decreased from 1.4×10^{-2} to 8.9×10^{-3} mA/cm^2 by introducing an Alq_3 layer. The decreased J_0 indicates a reduced recombination loss and an enhanced V_{oc}. As shown in Fig. 1(b), the lowest unoccupied molecular orbital (LUMO) level of NPB (−2.4 eV) is much higher than the conductance band edge of Sb_2Se_3, which can block the photo-generated electron diffusion from Sb_2Se_3 to ITO and then suppress the recombination near the anode. Meanwhile, the relatively low highest occupied molecular orbital (HOMO) level of Alq_3 means that it can resist the hole diffusion from Sb_2Se_3 to Al, and consequently reduce the recombination loss near the cathode. Figures 5(c) and 5(d) shows the characteristics of capacitance-frequency (C–f) and C^{-2}–V of the devices in the darkness. The capacitance of the device mainly comes from the junction, interface states, and bulk traps. At low frequency, all the interface states and bulk traps can vary with the alternating current (AC) signal applied. However, at higher frequencies, some interface states and bulk traps cannot be synchronized with the AC signal applied, and the measured capacitance will be decreased. As can be seen from Fig. 5(c), at lower frequencies, the capacitance of devices with an Alq_3

layer is smaller than that of the device without an Alq_3 layer, which indicates that the interface state density is decreased by introducing an Alq_3 layer (because the bulk trap densities were same). For the abrupt heterojunction, the relation between its capacitance and carrier density is as follows:

$$\frac{1}{C^2} = \frac{2\,(V_{\rm bi} - V)}{qA^2\varepsilon_0\varepsilon_r N_{\rm A}}, \tag{4}$$

where $V_{\rm bi}$ is the built-in potential, A is the device area, ε_0 is the vacuum permittivity, ε_r is the relative dielectric constant, and $N_{\rm A}$ is the carrier density. Figure 5(d) demonstrates the characteristics of C^{-2}–V at a frequency of 100 kHz for the devices with and without an Alq_3 layer. The $V_{\rm bi}$'s of 0.50 and 0.45 V for the devices with and without an Alq_3 layer were obtained from the intercept of the horizontal axis. The result indicates that $V_{\rm bi}$ can be improved by inserting an Alq_3 layer. In addition, we performed the TPV measurements to elucidate the photo-generated charge recombination dynamics, and the results are shown in Fig. 6. The device with an Alq_3 layer showed a longer carrier lifetime (7.8 µs) than that without an Alq_3 layer (5.1 µs). According to the above results, we can conclude that the introduction of the Alq_3 layer can reduce the interface state density, suppress charge recombination, and enhance the device performance.

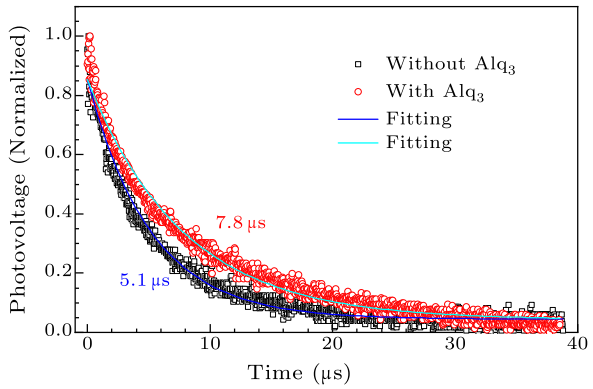

Fig. 6. Transient photovoltage decay curves of the device with and without an Alq_3 layer.

To further investigate the wavelength response of the device, we measured the EQE of the device. Figure 7 shows the EQE spectrum of an optimized device. The device demonstrated a wide photoelectric response spectrum, which extended to ∼1000 nm, in agreement with the band gap of Sb_2Se_3. The maximum EQE of 73% was achieved at 600 nm. There is a valley near 420 nm, which was caused by the effect of film interference. We derived the current density of 20.0 mA/cm^2 by integrating the EQE with the standard AM1.5 solar spectrum, which was very close to the value of 21.2 mA/cm^2 obtained from J–V measurement under the illumination from a solar simulator.

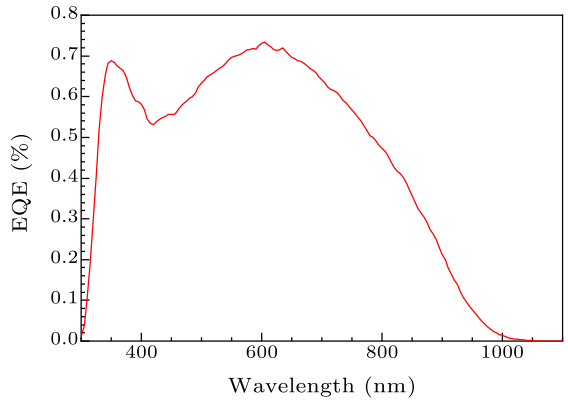

Fig. 7. EQE spectrum of the optimized device.

To investigate the repeatability of the devices, we fabricated 100 solar cells. The distribution of the PCEs is demonstrated in Fig. 8. The difference in PCE between devices is small, and the PCEs show a normal distribution with an average of 3.02% and a variance of 0.36%.

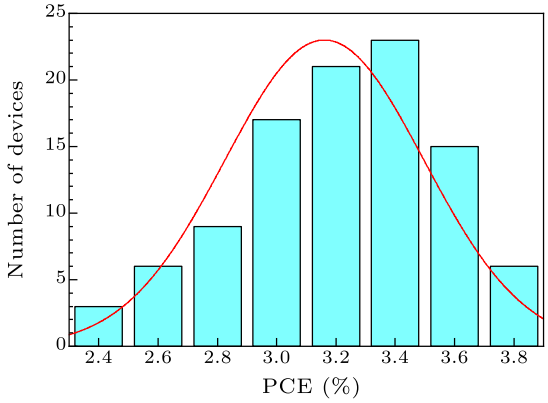

Fig. 8. Distribution of PCEs of 100 solar cells.

At present, $J_{\rm sc}$ of the Sb_2Se_3 film solar cells has reached a relatively high level. The lower $V_{\rm oc}$ is the main limited factor for the device performance. In all the reported results, the open circuit voltages are smaller than 0.5 V. In the future the three points below should be addressed to improve the $V_{\rm oc}$ of the device. (1) It is crucial to improve the crystal quality of the Sb_2Se_3 film and suppress the trap-assistant recombination. (2) The carrier mobilities are anisotropic in Sb_2Se_3 crystal. The carrier mobilities are the highest along the (001) direction. However, the preferred orientation is (020) in our film. The film with (001) preferred orientation is benefit for the device. (3) The $V_{\rm oc}$ is primarily determined by the Fermi level difference between Sb_2Se_3 and the n-type material. Therefore, higher $V_{\rm oc}$ can be obtained using the n-type material with a smaller work function. In addition, p-type doping can lower the Fermi level of the Sb_2Se_3, and consequently improve the $V_{\rm oc}$ of the cells.

In summary, Alq_3 was used as an electron transport layer in the Sb_2Se_3 film solar cell. The PCE

is increased by 72% by introducing an Alq_3 layer. The optimized device has a V_{oc} of 0.37 V, a J_{sc} of 21.2 mA/cm^2, and a PCE of 3.79%. A maximum EQE of 73% is achieved at 600 nm. The results suggest that adding an Alq_3 layer can reduce the interface state density, suppress the charge recombination, and consequently improve the device performance. This work provides a new electron transport material for Sb_2Se_3 film solar cells.

References

[1] Green M A, Hishikawa Y, Dunlop E D *et al.* 2018 *Prog. Photovoltaics* **26** 427
[2] Jackson P, Wuerz R, Hariskos D *et al.* 2016 *Phys. Status Solidi RRL* **10** 583
[3] Liu X, Chen J, Luo Met *et al.* 2014 *ACS Appl. Mater. & Interfaces* **6** 10687
[4] Chen C, Li W, Zhou Y *et al.* 2015 *Appl. Phys. Lett.* **107** 043905
[5] Zhou Y, Leng M, Xia Z *et al.* 2014 *Adv. Energy Mater.* **4** 1301846
[6] Voutsas G P, Papazoglou A G, Rentzeperis P J and Siapkas D 1985 *Z. Kristallogr.* **171** 261
[7] Luo M, Leng M, Liu X *et al.* 2014 *Appl. Phys. Lett.* **104** 173904
[8] Zhou Y, Wang L, Chen S *et al.* 2015 *Nat. Photon.* **9** 409
[9] Wen X, Chen C, Lu S *et al.* 2018 *Nat. Commun.* **9** 2179
[10] Kondrotas R, Zhang J, Wang C and Tang J 2019 *Sol. Energy Mater. Sol. Cells* **199** 16
[11] Liang G X, Zhang X H, Ma H L *et al.* 2017 *Sol. Energy Mater. Sol. Cells* **160** 257
[12] Liang G X, Zheng Z H, Fan P *et al.* 2018 *Sol. Energy Mater. Sol. Cells* **174** 263
[13] Hutter O S, Phillips L J, Durose K and Major J D 2018 *Sol. Energy Mater. Sol. Cells* **188** 177
[14] Li D B, Yin X, Grice C R *et al.* 2018 *Nano Energy* **49** 346
[15] Ngo T T, Chavhan S, Kosta I *et al.* 2014 *ACS Appl. Mater. & Interfaces* **6** 2836
[16] Choi Y C and Il S 2015 *Adv. Funct. Mater.* **25** 2892
[17] Choi Y C, Lee D U, Noh J H, Kim E K and Il S 2014 *Adv. Funct. Mater.* **24** 3587
[18] Choi Y C, Lee Y H, Im S H *et al.* 2014 *Adv. Funct. Mater.* **4** 1301680
[19] Wang W, Wang X, Chen G *et al.* 2018 *Sol. RRL* **2** 1800208
[20] Shi X, Zhang X, Tian Y, Shen C, Wang C and Gao H J 2012 *Appl. Surf. Sci.* **258** 2169
[21] Tang R, Wang X, Lian W *et al.* 2020 *Nat. Energy* **5** 587
[22] Messina S, Nair M T S and Nair P K 2009 *J. Electrochem. Soc.* **156** H327
[23] Leng M, Luo M, Chen C, Qin S *et al.* 2014 *Appl. Phys. Lett.* **105** 083905
[24] Li Z, Liang X, Li G, Liu H *et al.* 2019 *Nat. Commun.* **10** 125
[25] Shockley W and Queisser H J 1961 *J. Appl. Phys.* **32** 510
[26] Zhang L, Li Y, Li C *et al.* 2017 *ACS Nano* **11** 12753
[27] Polman A, Knight M, Garnett E C, Ehrler B and Sinke W C 2016 *Science* **352** aad4424
[28] Li G, Li Z, Liang X *et al.* 2019 *ACS Appl. Mater. & Interfaces* **11** 828
[29] Wu C, Jiang C, Wang X *et al.* 2019 *ACS Appl. Mater. & Interfaces* **11** 3207
[30] Wang L, Li D B, Li K *et al.* 2017 *Nat. Energy* **2** 17046
[31] Chen C, Zhao Y, Lu S *et al.* 2017 *Adv. Energy Mater.* **7** 1700866
[32] Lu S, Zhao Y, Chen C, Zhou Y *et al.* 2018 *Adv. Electron. Mater.* **4** 1700329
[33] Mihailetchi V D, Wildeman J and Blom P W M 2005 *Phys. Rev. Lett.* **94** 126602
[34] Koster L J A, Mihailetchi V D, Xie H and Blom P W M 2005 *Appl. Phys. Lett.* **87** 203502
[35] Chu T Y and Song O K 2007 *Appl. Phys. Lett.* **90** 203512
[36] Malliaras G G, Shen Y and Dunlap D H 2001 *Appl. Phys. Lett.* **79** 2582